# Chemical Imaging of Retinal Pigment Epithelium in Frozen Sections of Zebrafish Larvae Using ToF-SIMS

ACS Partner Journal

Journal of the American Society for Mass Spectrometry

pubs.acs.org/jasms

Research Article

# Chemical Imaging of Retinal Pigment Epithelium in Frozen Sections of Zebrafish Larvae Using ToF-SIMS

Sebastiaan Van Nuffel,* Khai C. Ang, Alex Y. Lin, and Keith C. Cheng

Cite This: *J. Am. Soc. Mass Spectrom.* 2021, 32, 255−261

Read Online

ACCESS | Metrics & More | Article Recommendations | Supporting Information

**ABSTRACT:** Variants of the *SLC24A5* gene, which encodes a putative potassium-dependent sodium−calcium exchanger (NCKX5) that most likely resides in the melanosome or its precursor, affect pigmentation in both humans and zebrafish (*Danio rerio*). This finding suggests that genetic variations influencing human skin pigmentation alter melanosome biogenesis via ionic changes. Gaining an understanding of how changes in the ionic environment of organelles impact melanosome morphogenesis and pigmentation will require a spatially resolved way to characterize the chemical environment of melanosomes in pigmented tissue such as retinal pigment epithelium (RPE). The imaging mass spectrometry technique most suited for this type of cell and tissue analysis is time-of-flight secondary ion mass spectrometry (ToF-SIMS) because it is able to detect many biochemical species with high sensitivity and with submicron spatial resolution. Here, we describe chemical imaging of the RPE in frozen-hydrated sections of larval zebrafish using cryo-ToF-SIMS. To facilitate the data interpretation, positive and negative polarity ToF-SIMS image data were transformed into a single hyperspectral data set and analyzed using principal component analysis. The combination of a novel protocol and the use of multivariate data analysis allowed us to discover new marker ions that are attributable to leucodopachrome, a metabolite specific to the biosynthesis of eumelanin. The described methodology may be adapted for the investigation of other classes of molecules in frozen tissues from zebrafish and other organisms.

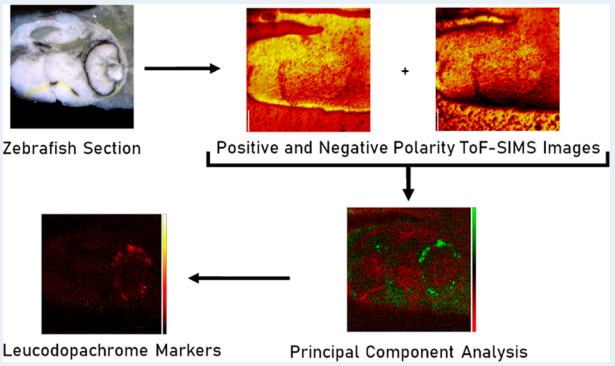


## INTRODUCTION

In the early 1980s, the zebrafish was developed as a vertebrate animal model suitable for genetic screens dedicated to the study of vertebrate development based on important experimental advantages as a model system.[1,2] The zebrafish (*Danio rerio*) is a robust, tropical freshwater schooling fish native to South Asia. Zebrafish breed on a year-round basis, and individual females can produce hundreds of offspring every few weeks. Because the fertilization and subsequent embryonic development are external, gametes can be harvested separately and genetically manipulated. Furthermore, zebrafish embryos are relatively large and optically transparent throughout their embryonic development, making studies of organ development tractable. The ease of creating embryonic mutations and screening for specific phenotypes and the short generation time have made the zebrafish one of the most important vertebrate model organisms for biological research. Wild-type strains are typically zebrafish from breeding populations with infrequently encountered phenotypic mutations, whereas mutant strains carry one or more randomly induced or targeted mutations and are maintained by selective breeding.[3]

Interestingly, one of the key skin pigmentation genes responsible for the lighter skin color of peoples of European lineage, the *SLC24A5* gene, also affects the pigmentation in the melanocytes and retinal pigmented epithelium (RPE) in the zebrafish *golden* (*gol*) mutant, which carries a nonsense mutation in *SLC24A5*. This gene encodes a putative potassium-dependent sodium/calcium exchanger (NCKX5) that localizes to an intracellular membrane, likely the melanosome or its precursor.[4] NCKX5 is postulated to modulate melanosome morphogenesis by changes in subcellular ionic compartments in conjunction with a proton pump and a proton−sodium exchanger, resulting in modification of both melanosome morphogenesis and pigment deposition. In humans, the hypomorphic *A111T* allele in the *SLC24A5* gene reduces the pigmentation up to 5 melanin units per mutant allele by decreasing the number of melanosomes per cell, their size, and the density and perhaps chemistry of melanin pigmentation. Null mutations in *SLC24A5* also causes a rare form of albinism in Asia now designated OCA6.[5] To determine how genetic variations in ion exchangers influence cellular pigmentation through changes in melanosome bio-

Received: August 10, 2020
Revised: September 26, 2020
Accepted: October 16, 2020
Published: October 28, 2020

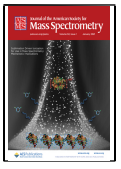

genesis, spatially resolved studies of the chemical environment of melanosomes are needed. We have used the wild-type zebrafish larval RPE as a model system to develop this ability.

Over the past two decades, imaging mass spectrometry (IMS) has proven to be a powerful tool to answer these kinds of research questions in biomedicine because it allows for label-free chemical imaging and provides molecular information.[6,7] Most biomolecular IMS studies involving zebrafish cross sections are matrix-assisted laser desorption/ionization (MALDI) or desorption electrospray ionization (DESI) IMS studies, which do not have the lateral resolution needed to image small features such as a layer of cells. Most of these studies have therefore been performed on dried whole-body[8−10] or brain tissue sections[11] of adult zebrafish. In 2015, Anderson et al. conducted a MALDI study to image ocular lens proteins of the zebrafish eyes with 80 $\mu$m spatial resolution.[12] However, there are a few publications where the RPE of other vertebrates has been visualized using MALDI IMS. In 2010, salamander retina phospholipids were investigated by Roy et al. using a 7 $\mu$m laser spot size.[13] In 2014, Anderson et al. imaged lipids in mouse retinal tissue with a laser spot size of 10 $\mu$m,[14] and in 2020, Anderson et al. investigated the lipid composition in human retina with a 10−15 $\mu$m pixel size.[15] However, we are interested in much smaller features for which we need a much better lateral resolution. Time-of-flight secondary ion mass spectrometry (ToF-SIMS) has the best spatial resolution of all the imaging mass spectrometry techniques for molecular imaging, and although more ion fragmentation occurs compared to MALDI or DESI, it can detect many biochemical compounds with high sensitivity.[16−18] ToF-SIMS can detect both inorganic and organic molecules, and it is sensitive enough to perform trace-element analyses. ToF-SIMS is a particularly good technique for imaging small organic molecules ($m/z$ < 2000) such as lipids and metabolites.[19,20] It also allows high spatial resolution imaging of non-native compounds such as drugs and toxins.[21,22] Using a typical ToF-SIMS setup, it is difficult to detect large molecules ($m/z$ > 2000) such as intact proteins or DNA/RNA, which tend to fragment into their amino acid and nucleobase building blocks.[23,24] However, successful peptide and protein imaging has recently been achieved using novel techniques such as matrix-enhanced SIMS[25] or argon gas cluster ion beam (GCIB) analysis guns.[26]

The lateral imaging resolution is constrained by the pixel size, which is dependent on the beam diameter of the analysis gun. The RPE layer we are trying to detect is a single cell layer, so the use of a ToF-SIMS instrument equipped with a Bi liquid metal ion gun (LMIG) is sensible because the LMIG has a spot size smaller than that of $C_{60}$ or Ar GCIBs and is capable of molecular imaging. The beam diameter of a typical Bi LMIG can be focused down to 1 $\mu$m in bunched mode while maintaining a high mass resolution and down to 200 nm in unbunched mode but with a reduced mass resolution.[27] ToF-SIMS is a chemical imaging technique with a lateral resolution comparable to that of a conventional optical microscope (~200 nm as determined by the Rayleigh criterion) and is thus capable of imaging single cells.[28] The subcellular precision of ToF-SIMS imaging makes it well suited for the investigation of the effect of calcium uptake into melanosomes, particularly in the RPE of zebrafish larvae, which are arranged peripherally around the outer globe of the zebrafish eye (see Figure 1). Furthermore, the Bi LMIG can be optimized for elemental imaging, which would be the next step in our study where we will compare $Ca^{2+}$ levels in the RPE between wild-type and *golden* mutant zebrafish. A small number of studies have used ToF-SIMS imaging to study zebrafish. In 2018, Kim et al. performed atmospheric pressure nanoparticle and plasma-assisted laser desorption/ionization (AP-nanoPALDI) and ToF-SIMS imaging experiments on adult zebrafish caudal fins to investigate molecular distribution changes that occur during their regeneration.[29] ToF-SIMS imaging has also been used to probe the role of lipids and metabolites in the disease states of zebrafish infected with *Mycobacterium marinum*, and a protocol was developed for dried whole-body cross sections of adult zebrafish with submicron resolution.[30−32] In addition, Kim et al. used ToF-SIMS to determine the calcium distribution in mouse retinal tissue in 2008.[33]

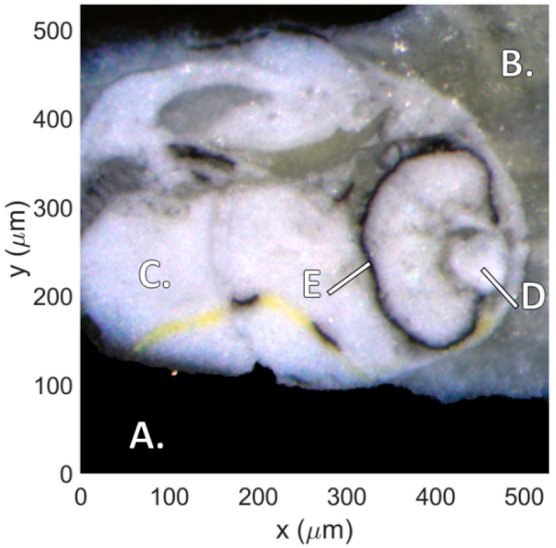


**Figure 1.** Reconstructed optical microscopy image (336×) of the freeze-dried zebrafish embryo's eye cross section that was investigated with ToF-SIMS in a frozen-hydrated state. We can clearly discern the ITO-coated glass substrate (A), the BSA matrix (B), the zebrafish tissue (C), the eye lens (D), and the black eye boundary caused by melanin in the retinal pigment epithelium (E).

The goals of this study were to find and visualize RPE-specific molecules in wild-type zebrafish larvae using ToF-SIMS imaging and to find basic methods that can be adopted for the broader application of ToF-SIMS to tissues of zebrafish or other small model organisms and specimens. A protocol was developed for cryo-ToF-SIMS measurements of frozen-hydrated eye cross sections of zebrafish larvae. We also demonstrated how positive and negative polarity ToF-SIMS image data can be transformed into a single hyperspectral data set that can be analyzed using principal component analysis (PCA) to reduce data complexity. The combination of this novel sample preparation protocol and the use of multivariate data analysis provided a way to identify marker ions of melanin-related molecules in larval retinal pigment epithelium.

## MATERIALS AND METHODS

**Zebrafish.** Wild-type Tübingen zebrafish were raised in the Penn State Functional Genomics Core. The male and female zebrafish were placed in the breeding tank in the afternoon prior to breeding while separated by a divider. The divider was removed in the morning of the day of breeding. Embryos were collected and sanitized using Ovadine solution (Syndel 25655-41-8). The embryos were raised in a Petri dish (50 embryos


https://dx.doi.org/10.1021/jasms.0c00300
J. Am. Soc. Mass Spectrom. 2021, 32, 255−261

per Petri dish) in an incubator with a temperature of 28 °C. Embryos were dechorionated at 3 days postfertilization prior to euthanasia using Tricaine-S (MS-222, Argent Chemical Laboratories).

**Substrates.** Using ultrasonic machining, 25 × 25 mm ITO-coated glass slides (576352 Sigma-Aldrich) were cut to 19 mm diameter circular disks in order to fit the cold stage of the PHI nanoTOF ToF-SIMS instrument.

**Sample Preparation.** Three-day-old wild-type zebrafish were aligned in 1% w/v low melting point (LM) agarose (Fisher BP160-500) blocks, which were prepared with 20% w/v bovine serum albumin (Sigma A4503) solution. Euthanized zebrafish larvae were embedded in agarose, as described in Sabaliauskas et al.[34] Phenol red (Sigma P0290) was added as a 1:4 mixture with 1% LM agarose and 20% BSA to fill the wells in order to act as a visual reference during cryo-sectioning. These blocks were then placed in cryomolds so that the zebrafish heads were facing up. The cryomolds were then filled with the same 1% LM agarose and 20% BSA mixture (see Supplementary Figure S1A).

The cryomolds were flash-frozen in liquid ethane, and the frozen blocks were stored in a −80 °C freezer.

A Leica cryostat microtome was used to cut 15−25 μm sections at −20 °C in order to obtain cross sections of a larvae's eye (see Supplementary Figure S1B). The tissue sections were thaw-mounted on conductive ITO-coated glass slides (19 mm diameter) and again stored in a −80 °C freezer.

**ToF-SIMS.** Cryo-SIMS measurements were executed using a PHI nanoTOF instrument (Physical Electronics, Chanhassen, MN, USA) equipped with a Bi LMIG and an Ar GCIB used as analysis and sputter gun, respectively, and were conducted at a temperature less than −145 °C (see Supplementary Figure S2) to prevent sublimation of the frozen-hydrated tissue sections in the vacuum of the analysis chamber.[35] The samples were kept in a frozen-hydrated state to prevent the migration of diffusible chemical species, which occurs during freeze-drying.[36] A nitrogen-gas-filled glovebox was fitted to the PHI nanoTOF instrument in order to prevent adsorption of moisture onto the sample during the sample mounting (see Supplementary Figure S3B).

Prior to chemical imaging, a 10 keV $Ar_{2000}^+$ cluster beam was used for sputtering a region of 900 × 900 μm at a current of 10 nA for 66 min to remove an ice layer that adsorbed itself to the sample during sample transfer. Charging of the sample was compensated with the low-energetic 25 eV electrons of the flood gun.

A 30 keV energy $Bi_3^+$ primary beam, operating at a DC current of 3.1 nA, was used to chemically image the frozen-hydrated zebrafish eye cross section in the positive and negative polarity. The primary ion beam was directed at the sample under an angle of 45° in relation to the normal and had a beam spot of 1−2 μm in the so-called high-current bunched mode. The primary ion beam was rastered at 512 × 512 pixels over a field of view of 600 × 600 μm; that is, the pixel size equals 1.2 μm. Twenty frames (1 shot per pixel) were collected for each image with a cycle time that allowed for a 0−1850 Da mass range. This resulted in an ion dose well below the static limit. Positive and negative polarity ToF-SIMS images were acquired separately at the same sample location. In the positive polarity, charging of the sample is compensated with PHI's dual-beam charge neutralization system using low-energetic 25 eV electrons of the flood gun and 200 V $Ar^+$ ions of the gas gun. In the negative polarity, charging of the sample is compensated with the low-energetic 25 eV electrons of the flood gun.

All positive spectra were internally calibrated using the same ions, namely, $CH_3^+$ at $m/z$ 15.0235, $H_3O^+$ at $m/z$ 19.0184, $H_5O_2^+$ at $m/z$ 37.0290, $H_7O_3^+$ at $m/z$ 55.0395, $H_9O_4^+$ at $m/z$ 73.0501, $H_{11}O_5^+$ at $m/z$ 91.0607, $H_{13}O_6^+$ at $m/z$ 109.0712, and $C_5H_{15}NPO_4^+$ at $m/z$ 184.0739 (phosphocholine headgroup). All negative spectra were internally calibrated using the same ions, namely, $CH^-$ at $m/z$ 13.0084, $CN^-$ at $m/z$ 26.0031, $H_3O_2^-$ at $m/z$ 35.0133, $CNO^-$ at $m/z$ 41.9980, $H_5O_3^-$ at $m/z$ 53.0239, $H_7O_4^-$ at $m/z$ 71.0344, and $C_{16}H_{31}O_2^-$ at $m/z$ 255.2324 (C16:0 FA).

**Microscopy.** After ToF-SIMS imaging, the stage cooling was halted and the sample was left overnight in the instrument's vacuum chamber to freeze-dry, which caused the sample to crack (see Supplementary Figure S4). This phenomenon is known to occur when the temperature rises too quickly during the freeze-drying process.[37] However, this does not interfere with the interpretation of the section. Optical microscopy images (336×) of the freeze-dried sample were acquired using a Zeiss SmartZoom 5. To remove the freeze-drying artifacts and thus improve the readability of the optical microscopy image, the image was realigned and registered manually, followed by adaptive region merging for manually selected areas to remove stitching lines (see Supplementary Figure S5).

**ToF-SIMS Data Analysis.** For ToF-SIMS data processing, a peak search was performed using the commercial PHI software (TOF-DR 3.0.0.13) to locate all major mass peaks. No deisotoping was performed. Secondary ion images were then exported in an BIF6 file format and imported into Matlab for further data processing with in-house generated Matlab scripts. The positive and negative polarity ion images are first normalized to the total number of ion counts per pixel and then digitally aligned to form a single hyperspectral image data set. Matching features between a positive polarity and a negative polarity ion image are manually selected to estimate the needed geometric transformation, which is solved for scale and angle and then applied to every individual ion image. Areas that are not present in both positive and negative polarity images are then cropped out. Standardized (autoscaled) PCA is then performed on this single hyperspectral image data set to facilitate the data analysis.[38] All calculations were performed on a 64-bit Windows 10 Pro platform with 64 GB of RAM, using an Intel Xeon E3-1545 M v5@2.90 GHz processor.

## RESULTS AND DISCUSSION

The reconstructed optical microscopy image shows the freeze-dried tissue embedded in the freeze-dried BSA matrix on top of the ITO-coated glass substrate (see Figure 1). Inside the tissue, we can clearly distinguish the dark RPE and the lens of the eye.

By converting the positive and negative polarity ion images (see Supplementary Figure S6) of the frozen-hydrated zebrafish eye cross section into a single hyperspectral image data set and performing PCA, we are able to identify positive and negative correlations between mass peaks from both polarities at the same time. The information obtained using PCA allows us to easily identify different chemistries. A scree plot determined that the first 13 PCs can be considered significant.

PC1 and PC2 allow us to distinguish the zebrafish tissue from the ITO-coated glass substrate and the BSA matrix. The score image of PC1 (see Supplementary Figure S7A) clearly


https://dx.doi.org/10.1021/jasms.0c00300
J. Am. Soc. Mass Spectrom. 2021, 32, 255−261

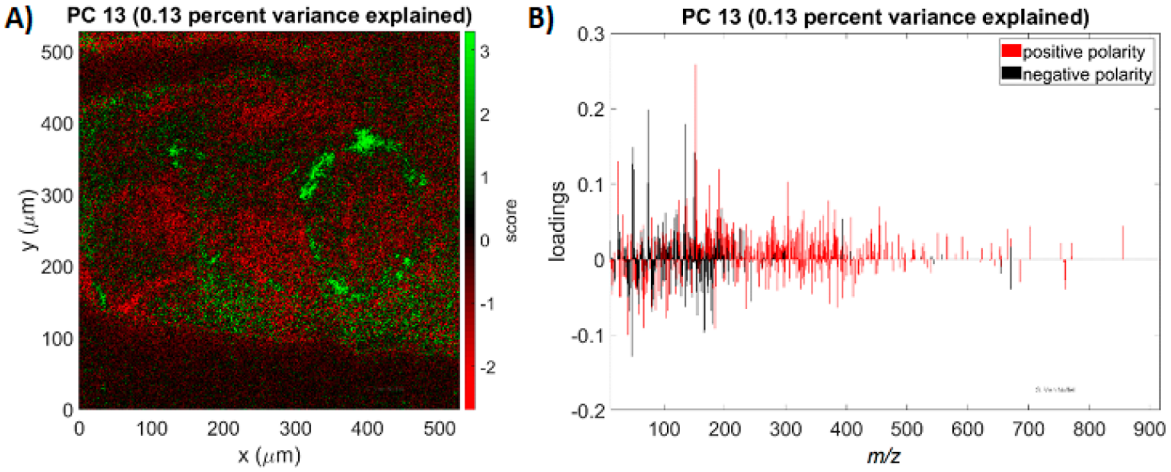


**Figure 2.** PCA of a single data set of positive and negative polarity ion images. (A) Score image of PC13 clearly distinguishes the RPE (green pixels) from the surrounding material (red pixels). (B) Positive loadings of PC13 contain known low-mass melanin markers such as $C_3N^-$ at $m/z$ 50.0, $C_3NO^-$ at $m/z$ 66.0, and $C_5N^-$ at $m/z$ 74.0 but also contain strong positive correlations for higher-mass ions at $m/z$ 152.07, 174.05, 190.03, and 303.13 in the positive polarity as well as an ion at $m/z$ 150.06 in the negative polarity.

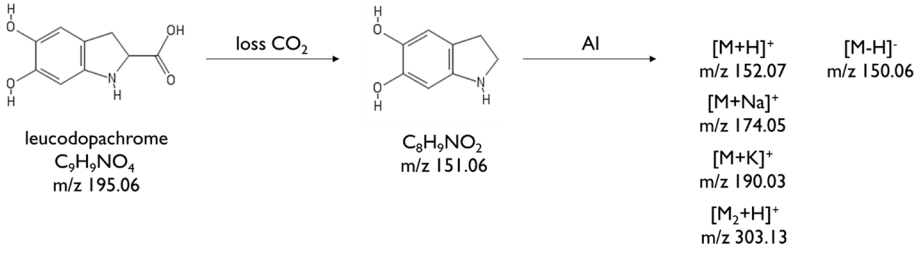


**Figure 3.** Proposed ion formation mechanism of $m/z$ 152.07, 174.05, 190.03, and 303.13 in the positive polarity as well as an ion at $m/z$ 150.06 in the negative polarity from leucodopachrome through neutral loss of $CO_2$ followed by adduct ionization.

distinguishes between the ITO substrate (green pixels) and the frozen material (red pixels). The positive loadings of PC1 (see Supplementary Figure S7B) contain repeating patterns of InO cluster ions such as $(InO)_nIn^+$ with $n$ = 0−6, $(InO)_nIn_2^+$ with $n$ = 0−4, $(InO)_nInO^-$ with $n$ = 0−4, $(InO)_nO^-$ with $n$ = 0−5, and $(InO)_nO_2^-$ with $n$ = 0−2, 4. The scores image of PC2 (see Supplementary Figure S7C) distinguishes the phospholipid signals originating from the tissue (green pixels) from the ice matrix (red pixels). The positive loadings of PC2 (see Supplementary Figure S7D) are characterized by typical phospholipid signals such as $C_5H_{15}NPO_4^+$ at $m/z$ 184.07 (phosphocholine headgroup) in the positive polarity and $PO_2^-$ at $m/z$ 62.96 and $PO_3^-$ at $m/z$ 78.96 in the negative polarity.[39] The negative loadings of PC2 contain repeating patterns of water cluster ions such as $(H_2O)_nH^+$ with $n$ = 0−20 in the positive polarity and $(H_2O)_nOH^-$ with $n$ = 0−12 in the negative polarity. Ion images of marker ions for ITO such as $In_3O_2^+$ and $In_3O_2^-$ at $m/z$ 376.70, phospholipids such as $C_5H_{15}NPO_4^+$ at $m/z$ 184.07 and $PO_3^-$ at $m/z$ 78.96, and ice such as $H_7O_3^+$ at $m/z$ 55.04 and $H_5O_3^-$ at $m/z$ 53.02 are shown in Supplementary Figure S8A−F). The ITO image is the negative of the ice image, which shows the sputtering successfully removed any adsorbed ice from the ITO substrate. The ice image partially overlaps with the phospholipids, which demonstrates the tissue is in a frozen-hydrated state. Areas with ice signals but no phospholipid signals correlate with the BSA matrix used to embed the zebrafish larvae. This proves the measurement is successful.

The positive loadings of PC7 (see Supplementary Figure S7F) contain salts such as $Na^+$ at $m/z$ 22.99 and $K^+$ at $m/z$ 38.96 but also various amino acid fragments such as $CN^-$ at $m/z$ 26.0 and $CNO^-$ at $m/z$ 42.0 in the negative polarity and $C_4H_8N^+$ at $m/z$ 70.07 (L,P,R) and $C_3H_7N_2O^+$ at $m/z$ 87.05 (G,N) in the positive polarity.[40] The ion images of $C_4H_8N^+$ at $m/z$ 70.07 and $C_3H_7N_2O^+$ at $m/z$ 87.05 are shown in Supplementary Figure S9A,B and show that the amino acids originate from both the tissue and the BSA matrix. Interestingly, there appears to be an increase of amino acid signal in one area. When the amino acid marker image is compared with the optical microscopy image (see Figure 1) of the sample after it was left to freeze-dry inside the instrument, it is clear the amino acid accumulation colocalizes with the eye lens, which is consistent with the literature. The vertebrate eye lens is rich in cytoplasmic protein because the eye lenses of vertebrates are composed of fiber cells arranged in concentric layers around a central nucleus.[41] As the new fiber cells develop, they express very high concentrations of Crystallin proteins, which are responsible for the high refractive index and transparency of the lens.[42] Lens Crystallins show high refractive index increments compared to other proteins due to large quantities of aromatic and sulfurous residues.[43] This is also observed in the ToF-SIMS data, which show intense signals for $C_8H_{10}N^+$ at $m/z$ 120.08 (F), $C_9H_8N^+$ at $m/z$ 130.06 (W), $C_8H_{10}NO^+$ at $m/z$ 136.08 (Y), and $C_2H_5S^+$ at $m/z$ 61.01 (M) in the eye lens.

For these studies, we were most interested in finding specific marker ions for the RPE. The score image of PC13 (see Figure


https://dx.doi.org/10.1021/jasms.0c00300
J. Am. Soc. Mass Spectrom. 2021, 32, 255−261

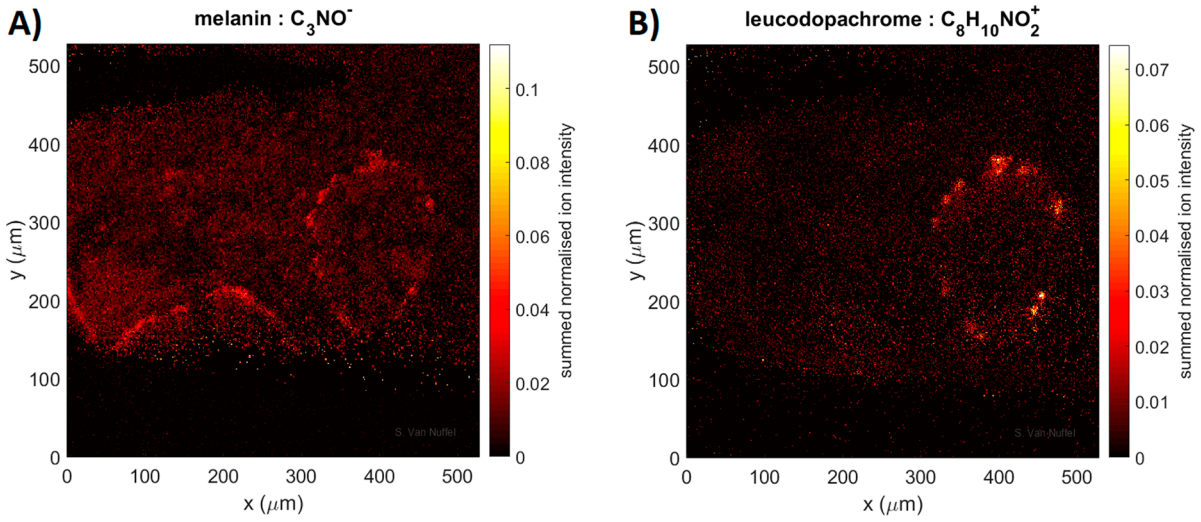


**Figure 4.** Ion images of marker ions for melanin and leucodopachrome. (A) Low-mass marker for melanin: $C_3NO^-$ at $m/z$ 66.0. (B) Pseudomolecular marker for leucodopachrome: $C_8H_{10}NO_2^+$ at $m/z$ 152.07.

2A) clearly distinguishes the RPE (green pixels), and the positive loadings of PC13 (see Figure 2B) contain known low-mass melanin markers such as $C_3N^-$ at $m/z$ 50.0, $C_3NO^-$ at $m/z$ 66.0, and $C_5N^-$ at $m/z$ 74.0.[44] Interestingly, the positive loadings for PC13 also contain strong positive correlations for higher-mass ions at $m/z$ 152.07, 174.05, 190.03, and 303.13 in the positive polarity as well as an ion at $m/z$ 150.06 in the negative polarity. All of these unreported higher-mass ions can be attributed to leucodopachrome, an intermediate in the biosynthesis of eumelanin.[45] The proposed ion formation is presented in Figure 3 and starts with the loss of $CO_2$ and is followed by various forms of adduct ionization. It is important to note that $C_8H_{10}NO_2^+$ at $m/z$ 152.07 and $C_8H_8NO_2^-$ at $m/z$ 150.06 are much more specific markers for the RPE compared to $C_3N^-$ at $m/z$ 50.0, $C_3NO^-$ at $m/z$ 66.0, and $C_5N^-$ at $m/z$ 74.0 that can originate from a variety of different parent molecules (see Figure 4 and Supplementary Figure S9C–E). This means the RPE can be visualized more precisely using pseudomolecular fragments indicative of an intermediate in the biosynthesis of eumelanin.

Finally, an overlay of marker ions for the various chemistries present in our zebrafish eye cross section is shown in Figure 5.

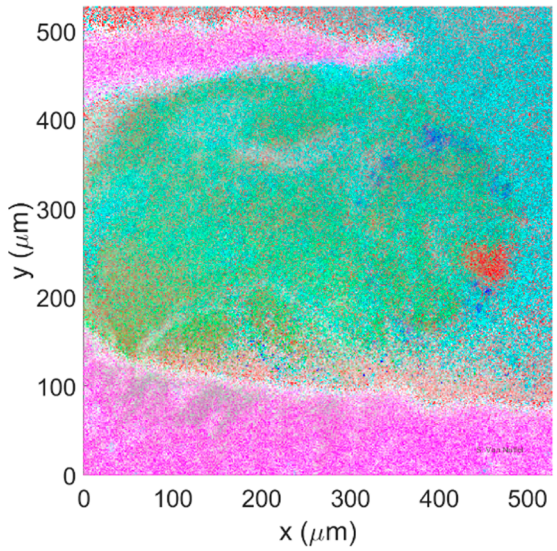


**Figure 5.** Overlay of the ToF-SIMS image data from the frozen zebrafish eye cross section. Different chemistries have been superimposed: ITO cluster ion signals (purple), water cluster ion signals (cyan), phospholipid markers (green), amino acid markers (red), and leucodopachrome markers (blue).

## CONCLUSION

We have successfully established a first protocol for cryo-ToF-SIMS measurements of frozen-hydrated zebrafish eye cross sections. This technique may be broadly applied to other tissues of zebrafish larvae and potentially other model organisms. Furthermore, we have shown that it is possible to identify positive and negative correlations between mass peaks from both polarities at the same time by converting the positive and negative polarity ion images into a single hyperspectral image data set and performing PCA. This type of data analysis greatly facilitates ToF-SIMS data interpretation and allowed us to identify new marker ions that are unique to the RPE. The discovered marker ions can be attributed to leucodopachrome, an intermediate in the biosynthesis of eumelanin, and can detect melanin-containing tissue with much greater specificity than the previously known low-mass marker ions for melanin. Importantly, it will now be possible to investigate the function of the *SLC24A5* gene by comparing the calcium uptake of the RPE between wild-type and mutant zebrafish larvae. Outside the bioimaging mass spectrometry community, our method will therefore be of great interest to anyone involved in melanocyte basic science research and the wider scientific community given the importance of the zebrafish as a model.

## ASSOCIATED CONTENT

### Supporting Information

The Supporting Information is available free of charge at https://pubs.acs.org/doi/10.1021/jasms.0c00300.

Figures S1–S9 (PDF)

## AUTHOR INFORMATION

### Corresponding Author

**Sebastiaan Van Nuffel** – *Materials Research Institute, The Pennsylvania State University, University Park, Pennsylvania*



https://dx.doi.org/10.1021/jasms.0c00300
*J. Am. Soc. Mass Spectrom.* 2021, 32, 255–261

*16802, United States;* orcid.org/0000-0003-1251-3236; Email: sebastiaan.vannuffel@psu.edu

### Authors

**Khai C. Ang** – *The Jake Gittlen Laboratories for Cancer Research, Division of Experimental Pathology, Department of Pathology, and Penn State Zebrafish Functional Genomics Core, Penn State College of Medicine, Hershey, Pennsylvania 17033, United States;* orcid.org/0000-0001-7695-9953

**Alex Y. Lin** – *The Jake Gittlen Laboratories for Cancer Research, Division of Experimental Pathology, Department of Pathology, and Penn State Zebrafish Functional Genomics Core, Penn State College of Medicine, Hershey, Pennsylvania 17033, United States;* orcid.org/0000-0002-1653-4168

**Keith C. Cheng** – *The Jake Gittlen Laboratories for Cancer Research, Division of Experimental Pathology, Department of Pathology, and Penn State Zebrafish Functional Genomics Core, Penn State College of Medicine, Hershey, Pennsylvania 17033, United States;* orcid.org/0000-0002-5350-5825

Complete contact information is available at: https://pubs.acs.org/10.1021/jasms.0c00300

### Author Contributions

S.V.N. performed cryo-ToF-SIMS experiments and data analysis and wrote the main manuscript. K.A. and A.L. prepared and cryo-sectioned the zebrafish samples. K.C. proposed and designed the study with S.V.N. and K.A. The manuscript was written with contributions from all authors. All authors have given approval to the final version of the manuscript.

### Notes

The authors declare no competing financial interest.

Ethics approval: IACUC approval for this experiment is PRAMS201646733.

## ■ ACKNOWLEDGMENTS

This work was supported by a pilot grant from the Pennsylvania State University's Institute for Cyberscience (ICS), renamed the Institute for Computational and Data Science (ICDSm). The authors would also like to thank the Pennsylvania State University's Materials Research Institute (MRI), Department of Pathology, Jake Gittlen Laboratories for Cancer Research, and the Zebrafish Functional Genomics Core at the College of Medicine for funding and support as well as the Pennsylvania Tobacco Funds and the Jake Gittlen Memorial Golf Tournament. In addition, we would like to thank Manuel Villalpando (MCL, Pennsylvania State University) for the ultrasonic machining of the sample substrates, Dr. Matthew Swulius (Department of Biochemistry and Molecular Biology, College of Medicine, Pennsylvania State University) for supplying cryogenics used to flash-freeze the tissue blocks, Dr. Ryan Hobbs (Department of Dermatology, College of Medicine, Pennsylvania State University) for the use of his lab's cryostat microtome, John Cantolina and Missy Hazen (Huck, Pennsylvania State University) for assisting with cryo-sectioning, as well as Vincent Bojan (MCL, Pennsylvania State University) for assisting with cryo-ToF-SIMS measurements. We would also like to thank Dr. Greg Fisher (PHI) and Dr. Jordan Lerach for useful discussions regarding cryo-ToF-SIMS measurements as well as Prof. Nicholas Winograd (Department of Chemistry, Pennsylvania State University). We would like to thank Dr. Anna Madra (Department of Civil and Environmental Engineering, Pennsylvania State University) for digital stitching and processing of microscopy images of the sample.

## ■ REFERENCES

(1) Streisinger, G.; Walker, C.; Dower, N.; Knauber, D.; Singer, F. Production of clones of homozygous diploid zebra fish (Brachydanio rerio). *Nature* **1981**, *291*, 293–296.

(2) Nusslein-Volhard, C.; Dahm, R. *Zebrafish.*; Oxford University Press, 2002.

(3) Trevarrow, B.; Robison, B. Genetic Backgrounds, Standard Lines, and Husbandry of Zebrafish. *Methods in Cell Biology*; Academic Press, 2004; pp 599–616.

(4) Lamason, R. L.; Mohideen, M. A. P.; Mest, J. R.; Wong, A. C.; Norton, H. L.; Aros, M. C.; Jurynec, M. J.; Mao, X.; Humphreville, V. R.; Humbert, J. E.; Sinha, S.; Moore, J. L.; Jagadeeswaran, P.; Zhao, W.; Ning, G.; Makalowska, I.; McKeigue, P. M.; O'donnell, D.; Kittles, R.; Parra, E. J.; Mangini, N. J.; Grunwald, D. J.; Shriver, M. D.; Canfield, V. A.; Cheng, K. SLC24A5, a putative cation exchanger, affects pigmentation in zebrafish and humans. *Science* **2005**, *310*, 1782–1786.

(5) Wei, A.-H.; Zang, D.-J.; Zhang, Z.; Liu, X.-Z.; He, X.; Yang, L.; Wang, Y.; Zhou, Z.-Y.; Zhang, M.-R.; Dai, L.-L.; Yang, X.-M.; Li, W. Exome sequencing identifies SLC24A5 as a candidate gene for nonsyndromic oculocutaneous albinism. *J. Invest. Dermatol.* **2013**, *133*, 1834–1840.

(6) Heeren, R. M. A.; McDonnell, L. A.; Amstalden, E.; Luxembourg, S. L.; Altelaar, A. F. M.; Piersma, S. R. Why don't biologists use SIMS? A critical evaluation of imaging MS. *Appl. Surf. Sci.* **2006**, *252*, 6827–6835.

(7) Gilmore, I. S.; Heiles, S.; Pieterse, C. L. Metabolic imaging at the single-cell scale: recent advances in mass spectrometry imaging. *Annu. Rev. Anal. Chem.* **2019**, *12*, 201–224.

(8) Stutts, W. L.; Knuth, M. M.; Ekelöf, M.; Mahapatra, D.; Kullman, S. W.; Muddiman, D. C. Methods for Cryosectioning and Mass Spectrometry Imaging of Whole-Body Zebrafish. *J. Am. Soc. Mass Spectrom.* **2020**, *31*, 768–772.

(9) Perez, C. J.; Tata, A.; de Campos, M. L.; Peng, C.; Ifa, D. R. Monitoring toxic ionic liquids in zebrafish (Danio rerio) with desorption electrospray ionization mass spectrometry imaging (DESI-MSI). *J. Am. Soc. Mass Spectrom.* **2017**, *28*, 1136–1148.

(10) Nelson, K. A.; Daniels, G. J.; Fournie, J. W.; Hemmer, M. J. Optimization of whole-body zebrafish sectioning methods for mass spectrometry imaging. *J. Biomol. Technol.* **2013**, *24*, 119.

(11) Villacrez, M.; Hellman, K.; Ono, T.; Sugihara, Y.; Rezeli, M.; Ek, F.; Marko-Varga, G.; Olsson, R. Evaluation of drug exposure and metabolism in locust and zebrafish brains using mass spectrometry imaging. *ACS Chem. Neurosci.* **2018**, *9*, 1994–2000.

(12) Anderson, D. M.; Floyd, K. A.; Barnes, S.; Clark, J. M.; Clark, J. I.; Mchaourab, H.; Schey, K. L. A method to prevent protein delocalization in imaging mass spectrometry of non-adherent tissues: application to small vertebrate lens imaging. *Anal. Bioanal. Chem.* **2015**, *407*, 2311–2320.

(13) Roy, M. C.; Nakanishi, H.; Takahashi, K.; Nakanishi, S.; Kajihara, S.; Hayasaka, T.; Setou, M.; Ogawa, K.; Taguchi, R.; Naito, T. Salamander retina phospholipids and their localization by MALDI imaging mass spectrometry at cellular size resolution. *J. Lipid Res.* **2011**, *52*, 463–470.

(14) Anderson, D. M.; Ablonczy, Z.; Koutalos, Y.; Spraggins, J.; Crouch, R. K.; Caprioli, R. M.; Schey, K. L. High resolution MALDI imaging mass spectrometry of retinal tissue lipids. *J. Am. Soc. Mass Spectrom.* **2014**, *25*, 1394–1403.

(15) Anderson, D. M.; Messinger, J. D.; Patterson, N. H.; Rivera, E. S.; Kotnala, A.; Spraggins, J. M.; Caprioli, R. M.; Curcio, C. A.; Schey, K. L. Lipid Landscape of the Human Retina and Supporting Tissues Revealed by High Resolution Imaging Mass Spectrometry. *J. Am. Soc. Mass Spectrom.* **2020**, DOI: 10.1021/jasms.0c00119.

(16) Bich, C.; Touboul, D.; Brunelle, A. Biomedical studies by TOF-SIMS imaging. *Biointerphases* **2015**, *10*, 018901.
(17) Fearn, S. Characterisation of biological material with ToF-SIMS: a review. *Mater. Sci. Technol.* **2015**, *31*, 148−161.
(18) Massonnet, P.; Heeren, R. M. A concise tutorial review of TOF-SIMS based molecular and cellular imaging. *J. Anal. At. Spectrom.* **2019**, *34*, 2217−2228.
(19) Gilmore, I. S. SIMS of organics—Advances in 2D and 3D imaging and future outlook. *J. Vac. Sci. Technol., A* **2013**, *31*, 050819.
(20) Bich, C.; Touboul, D.; Brunelle, A. Cluster TOF-SIMS imaging as a tool for micrometric histology of lipids in tissue. *Mass Spectrom. Rev.* **2014**, *33*, 442−451.
(21) Passarelli, M. K.; Newman, C. F.; Marshall, P. S.; West, A.; Gilmore, I. S.; Bunch, J.; Alexander, M. R.; Dollery, C. T. Single-cell analysis: visualizing pharmaceutical and metabolite uptake in cells with label-free 3D mass spectrometry imaging. *Anal. Chem.* **2015**, *87*, 6696−6702.
(22) Desbenoit, N.; Schmitz-Afonso, I.; Baudouin, C.; Laprévote, O.; Touboul, D.; Brignole-Baudouin, F.; Brunelle, A. Localisation and quantification of benzalkonium chloride in eye tissue by TOF-SIMS imaging and liquid chromatography mass spectrometry. *Anal. Bioanal. Chem.* **2013**, *405*, 4039−4049.
(23) Salter, T. L.; Green, F. M.; Gilmore, I. S.; Seah, M. P.; Stokes, P. A comparison of SIMS and DESI and their complementarities. *Surf. Interface Anal.* **2011**, *43*, 294−297.
(24) Lhoest, J. B.; Wagner, M. S.; Tidwell, C. D.; Castner, D. G. Characterization of adsorbed protein films by time of flight secondary ion mass spectrometry. *J. Biomed. Mater. Res.* **2001**, *57*, 432−440.
(25) Ogrinc Potočnik, N.; Fisher, G. L.; Prop, A.; Heeren, R. M. Sequencing and identification of endogenous neuropeptides with matrix-enhanced secondary ion mass spectrometry tandem mass spectrometry. *Anal. Chem.* **2017**, *89*, 8223−8227.
(26) Son, J. G.; Yoon, S.; Shon, H. K.; Moon, J. H.; Joh, S.; Lee, T. G. Ar-gas cluster ion beam in ToF-SIMS for peptide and protein analysis. *Biointerphases* **2020**, *15*, 021011.
(27) Sodhi, R. N. Time-of-flight secondary ion mass spectrometry (TOF-SIMS): —versatility in chemical and imaging surface analysis. *Analyst* **2004**, *129*, 483−487.
(28) Van Nuffel, S.; Parmenter, C.; Scurr, D. J.; Russell, N. A.; Zelzer, M. Multivariate analysis of 3D ToF-SIMS images: method validation and application to cultured neuronal networks. *Analyst* **2016**, *141*, 90−95.
(29) Kim, J. Y.; Lee, S. Y.; Kim, H.; Park, J. W.; Lim, D. K.; Moon, D. W. Biomolecular imaging of regeneration of zebrafish caudal fins using high spatial resolution ambient mass spectrometry. *Anal. Chem.* **2018**, *90*, 12723−12730.
(30) Fisher, G. L.; Bruinen, A. L.; Ogrinc Potočnik, N.; Hammond, J. S.; Bryan, S. R.; Larson, P. E.; Heeren, R. M. A new method and mass spectrometer design for TOF-SIMS parallel imaging MS/MS. *Anal. Chem.* **2016**, *88*, 6433−6440.
(31) Bruinen, A. L.; Fisher, G. L.; Heeren, R. M. ToF-SIMS parallel imaging MS/MS of lipid species in thin tissue sections. *Imaging Mass Spectrometry*; Humana Press: New York, 2017; pp 165−173.
(32) Bruinen, A. L.; Fisher, G. L.; Balez, R.; van der Sar, A. M.; Ooi, L.; Heeren, R. M. Identification and High-Resolution Imaging of α-Tocopherol from Human Cells to Whole Animals by TOF-SIMS Tandem Mass Spectrometry. *J. Am. Soc. Mass Spectrom.* **2018**, *29*, 1571−1581.
(33) Kim, J. H.; Kim, J. H.; Ahn, B. J.; Park, J. H.; Shon, H. K.; Yu, Y. S.; Moon, D. W.; Lee, T. G.; Kim, K. W. Label-free calcium imaging in ischemic retinal tissue by TOF-SIMS. *Biophys. J.* **2008**, *94*, 4095−4102.
(34) Sabaliauskas, N. A.; Foutz, C. A.; Mest, J. R.; Budgeon, L. R.; Sidor, A. T.; Gershenson, J. A.; Joshi, S. B.; Cheng, K. C. High-throughput zebrafish histology. *Methods* **2006**, *39*, 246−254.
(35) Linner, J. G.; Livesey, S. A.; Harrison, D. S.; Steiner, A. L. A new technique for removal of amorphous phase tissue water without ice crystal damage: a preparative method for ultrastructural analysis and immunoelectron microscopy. *J. Histochem. Cytochem.* **1986**, *34*, 1123−1135.
(36) Angerer, T. B.; Fletcher, J. S. 3D Imaging of TiO2 nanoparticle accumulation in Tetrahymena pyriformis. *Surf. Interface Anal.* **2014**, *46*, 198−203.
(37) Bell, L. G. E. Freeze-Drying. In *Physical Techniques in Biological Research*; Oster, G., Pollister, A. W., Eds.; Elsevier, 2013; pp 1−27.
(38) Van Nuffel, S.; Elie, N.; Yang, E.; Nouet, J.; Touboul, D.; Chaurand, P.; Brunelle, A. Insights into the MALDI process after matrix deposition by sublimation using 3D ToF-SIMS imaging. *Anal. Chem.* **2018**, *90*, 1907−1914.
(39) Passarelli, M. K.; Winograd, N. Lipid imaging with time-of-flight secondary ion mass spectrometry (ToF-SIMS). *Biochim. Biophys. Acta, Mol. Cell Biol. Lipids* **2011**, *1811*, 976−990.
(40) Wagner, M. S.; Castner, D. G. Characterization of adsorbed protein films by time-of-flight secondary ion mass spectrometry with principal component analysis. *Langmuir* **2001**, *17*, 4649−4660.
(41) Moreau, K. L.; King, J. A. Protein misfolding and aggregation in cataract disease and prospects for prevention. *Trends Mol. Med.* **2012**, *18*, 273−282.
(42) Aarts, H. J.; Lubsen, N. H.; Schoenmakers, J. G. Crystallin gene expression during rat lens development. *Eur. J. Biochem.* **1989**, *183*, 31−36.
(43) Mahendiran, K.; Elie, C.; Nebel, J. C.; Ryan, A.; Pierscionek, B. K. Primary sequence contribution to the optical function of the eye lens. *Sci. Rep.* **2014**, *4*, 5195.
(44) Lindgren, J.; Uvdal, P.; Sjövall, P.; Nilsson, D. E.; Engdahl, A.; Schultz, B. P.; Thiel, V. Molecular preservation of the pigment melanin in fossil melanosomes. *Nat. Commun.* **2012**, *3*, 824.
(45) Yamaguchi, Y.; Hearing, V. J.; Maeda, A.; Morita, A. NADPH: quinone oxidoreductase-1 as a new regulatory enzyme that increases melanin synthesis. *J. Invest. Dermatol.* **2010**, *130*, 645−647.


https://dx.doi.org/10.1021/jasms.0c00300
*J. Am. Soc. Mass Spectrom.* 2021, 32, 255−261